Rearrangement dynamics of fishbonelike Turing patterns generated by spatial periodic forcing

Tamás Bánsági, Jr., Sama Ansari, Irving R. Epstein, and Milos Dolnik
Department of Chemistry and Volen Center for Complex Systems, MS 015, Brandeis University, Waltham, Massachusetts 02454-9110, USA
(Received 2 March 2010; published 11 June 2010)

External forcing can greatly affect the evolution of Turing patterns in reaction-diffusion (RD) media. Here, we employ spatially periodic illumination in a photosensitive RD system to create Turing structures that are repetitive in one direction. We then study their relaxation in the absence of light. These unforced, fishbonelike configurations undergo self-reorganization and establish stationary arrangements, some of which fully exhibit, while others partially or completely lose, the symmetry of the initially imposed pattern.

DOI: 10.1103/PhysRevE.81.066207 PACS number(s): 82.40.Bj, 82.40.Ck, 47.54.−r, 89.75.Fb

I. INTRODUCTION

The reaction-diffusion (RD) theory of morphogenesis, proposed by Alan Turing [1] more than half a century ago, has generated considerable interest in the scientific community, as he demonstrated that via a diffusion-driven instability spatially periodic, temporally stationary patterns, now referred to as Turing patterns (TP), can emerge. Early studies focused on biological applications, but the first experimental evidence of such instability [2] was obtained in a chemical system, the chlorite–iodide–malonic acid (CIMA) reaction [3].

This reaction and its modified version, the CDIMA [4] reaction, involving chlorine dioxide and iodine to replace chlorite and iodide, respectively, have been widely employed in last 20 years to study TP. The photosensitivity of the CDIMA reaction has been utilized to study the effect of external spatial-temporal forcing on TP. Constant uniform illumination affects the characteristics of TP and suppresses them at higher intensities [5]. Spatially uniform but temporally periodic illumination has a similar effect [6]. Spatially periodic forcing was found to interact with Turing structures, modifying their symmetry and wavelength [7] and facilitating the formation of hexagonal and square superlattice structures [8,9]. Spatiotemporal periodic forcing can also lead to a variety of dynamics, ranging from oscillating hexagons and waving stripes [10] to unique pattern growth scenarios [11].

Illumination of TP has been successfully applied to imprint simple, striped TP with wavelengths different from the intrinsic wavelength [12], provided that the light intensity is sufficiently high. When the illumination is removed, the imprinted patterns undergo self-rearrangement to establish stationary configurations. The resulting patterns are composed of stripes with the same orientation imposed during imprinting when the wavelength of forcing is close to the natural wavelength or small even multiples, e.g., twice or four times the natural wavelength. Otherwise, the pattern zigzags or contains mixtures of stripes and labyrinthine domains. The orientation of the stripes in these asymmetric patterns depends on the wavelength of the forcing.

Such periodic initial layouts, however, are far less complex than naturally occurring labyrinthine TP, which contain defects such as kinks, junctions, segmented and circular stripes. These types of imperfections are not limited to reactive systems. Similar defects have been seen in Rayleigh-Bénard convection patterns [13] and in thin films of self-assembling, nano-meter-scale block copolymers [14].

Here, in order to study the self-rearrangement of TP emerging from more complex initial conditions, we imprint fishbonelike TP of parallel stripes, each with a kink at the same position, and follow their relaxation. Investigating these configurations, which resemble segments of superlattice patterns along a line of vertices, may be useful in designing new types of superlattice TP.

II. EXPERIMENTAL

The pattern formation takes place in a one-sided continuously fed unstirred reactor (CFUR) made from a 2%, 0.45 mm thick, 38 mm diameter agarose (Fluka) gel. The CFUR is mounted between an impermeable glass window and a continuously fed stirred tank reactor (CSTR), which serves as a feeding chamber. Two membranes separate the reactors, a cellulose nitrate membrane (Whatman, pore size 0.45 μm, thickness 0.12 mm), which enhances contrast and, underneath it, an anopore membrane (Whatman, pore size 0.2 μm, impregnated with 4% agarose gel, overall thickness 0.10 mm) inserted to provide rigidity to the CFUR and separation from the turbulent flow in the adjoining, vigorously stirred CSTR. The CFUR-CSTR assembly is submerged in a temperature-controlled water bath during the course of the reaction and thermostated at 4 °C.

We feed solutions of iodine (Fisher Scientific), malonic acid (MA, Sigma-Aldrich) mixed with poly-(vinyl alcohol) (PVA, Sigma-Aldrich, average molecular weight 9000–10000), and chlorine dioxide, prepared as described in Ref. [15], into the CSTR using peristaltic pumps (Rainin). The role of PVA is twofold: it serves as a binding agent and also as a color indicator. It forms a complex with tri-iodide ions, diminishing the effective diffusivity of iodine, which is necessary for Turing patterns to develop. Each solution contains 10 mM sulfuric acid (Fisher Scientific). Upon mixing in the CSTR, the initial concentrations in the feeding chamber are: $[I_2]=0.3$ mM, $[MA]=1.8$ mM, $[ClO_2]=0.14$ mM, $[PVA]=10$ g/l, unless otherwise indicated. The residence time of the reagents in the CSTR is 160 s.

For illumination we use a video projector (NEC VT 770) controlled by a PC. A biconvex lens and a neutral density

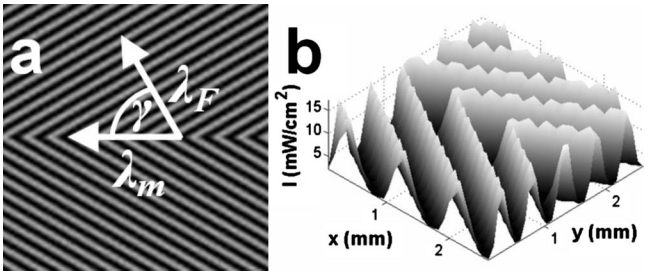

FIG. 1. A mask for spatial periodic forcing of Turing patterns (a) and its calculated intensity map upon projection onto the working medium (b). Vectors represent the primary directions of periodicity with wavelengths λ_F and λ_m. λ_m is a function of the rotation angle γ and λ_F. Intensity surface is chipped due to numerical rounding.

filter (with 59% transmittance) are placed in the light path. The former focuses the divergent rays of light produced by the projector to cast a smaller and brighter image onto the CFUR mounted precisely in the image plane of the lens. The latter is utilized to offset the increase in light intensity.

We project eight-bit grayscale images, as masks, onto the working medium. They consist of two sets of parallel lines with wavelength (λ_F) that meet at an angle π-2γ [Fig. 1(a)]. This generates a periodic pattern with wavelength λ_m along the axis of symmetry where the lines meet, with $\lambda_m = \lambda_F/\cos(\gamma)$, where γ is the angle between the two primary directions of periodicity. We measure the light intensity for different gray levels at the CFUR with a power meter (Newport 1815-C) and calculate intensity maps for the projected masks [Fig. 1(b)].

A camera (Pulnix) equipped with a Hamamatsu camera control unit is used to acquire monochrome images. Snapshots of TP are taken in ambient light, with no image cast on the CFUR, at a light intensity of 0.6 mW/cm^2.

III. EXPERIMENTAL RESULTS

After commencing feeding and submerging the reactor in the temperature controlled water bath, we allow approximately 2 h for TP to form spontaneously. Then we take a snapshot and compute the Fourier spectrum of the TP to evaluate the wavelength of the natural pattern, λ_P. In agreement with earlier studies [12], we find $\lambda_P = 0.45 \pm 0.02$ mm.

The spontaneously developed TP are then illuminated with strong uniform white light (32 mW/cm^2) for 5 min. Due to photodissociation [1], the iodine concentration and, consequently, the concentration of the triiodide-PVA complex diminishes in the CFUR, resulting in a uniform, colorless state, which appears white owing to the color of the cellulose nitrate membrane beneath. Once the strong illumination is turned off, in only ambient light, the system begins to recover. The iodine concentration replenishes itself and, as it increases, we see a gradual color change in the gel caused by the concurrent growth of the triiodide-PVA concentration. Eventually, a dark (high-triiodide-PVA) state emerges, accompanied by randomly distributed white spots, which serve as germs of a TP.

In this study, we control the system's recovery process by projecting images (Fig. 1) onto the working medium after the suppression. The development of TP depends on the specific geometry of the mask imposed and on the light intensity. In all experiments we keep the maximum light intensity of projected images constant at 16 mW/cm^2 (the minimum light intensity is 0) and vary the forcing wavelength λ_F and the angle γ. These variable parameters define two wavelength ratios: $R = \lambda_F/\lambda_P$ and $R_m = \lambda_m/\lambda_P$. Each image is cast on the CFUR for 20 min, enough time for the pattern to become stationary. Snapshots of relaxing TP are then taken for at least 1 h. Within this time period, the TP become more or less stationary and there is no further visible change in these patterns.

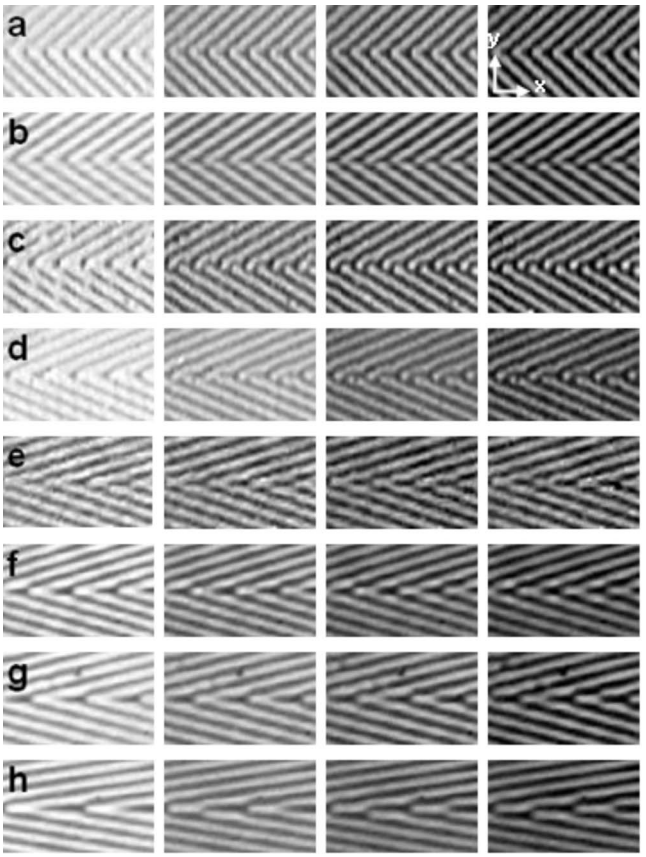

FIG. 2. Pattern development following spatial periodic forcing by illumination; $R=1.0$, (a) $R_m=1.5$, (b) $R_m=1.75$, (c) $R_m=2.0$, (d) $R_m=2.6$, (e) $R_m=3.0$, (f) $R_m=3.5$, (g) $R_m=4.0$, and (h) $R_m=6.0$. Snapshots in each row are taken 0, 10, 30, and 60 min after the light is turned off. Image size: 5×3 mm^2.

As shown previously [2], for R near unity, TP align with the striped forcing mask and remain stationary. In our study we begin with the simplest scenario, in which $R=1.0$ and the angle γ is the only variable parameter. We first focus on the effect of the different forcing wavelengths along the symmetry axis. Experimental results for $R=1.0$ and $6.0 \geq R_m \geq \sqrt{2}$ are shown in Fig. 2. Each row displays snapshots from a 60 min relaxation period, which begins immediately after the illumination is turned off. The snapshots in the first column are always brighter than the subsequent ones, because the iodine concentration is below its natural level in both the low-I_2 (bright) and high-I_2 (dark) domains of the TP. In the first column of snapshots, taken immediately after the illu-

mination is switched off, we see that the TP have aligned with the corresponding masks (not shown) both along the symmetry axis and elsewhere. Then the patterns undergo a self-rearrangement that may result in new structures favored over the imposed configurations. The study of transient patterns and their reorganization is not the subject of the present work, as we focus on the variety of attainable static geometries that arise from our forced fishbonelike initial arrangements.

After the illumination is turned off, the TP remain unchanged away from the axis, in agreement with previous experiments using striped masks with $R=1.0$ [12]. Besides the apparent adjustment in amplitude, we observe no other change as these patterns are already in a stable arrangement.

Along the line of vertices, the self-rearrangement may alter the patterns produced by forcing, since R_m is greater than unity in all cases, i.e., $\lambda_F/\lambda_m<1$. We see, however, that most of the TP preserve their configuration established during illumination. Even for wavelength ratios in the range $\sqrt{2}\leq R_m\leq 1.64$ ($45.0°\leq\gamma\leq 52.5°$), where one would expect a symmetry loss based on previous studies using striped masks, the imprinted patterns remain virtually unchanged throughout the relaxation process [Fig. 2(a)]. There is only a slight adjustment along the symmetry axis in which the bright vertices transform into small nibs. In contrast, very different patterns are formed when using simple striped masks with the same wavelength ratio [12]. TP become unstable shortly after the illumination is turned off, and the imposed bands zigzag ($R=1.4$) or break ($R=1.6$). In the case of fully developed square superlattices, where $R_m=\sqrt{2}$ as well in the diagonal direction, TP become slightly distorted [8]. Considering the persistence of the imposed arrangement we observe in the horizontal midsection here, the deformation in the superlattice configuration can be attributed to the increased stress present at the core of the superlattice cells. The instability in the fishbone structure, which takes the form of splittings along the symmetry axis [Fig. 2(b)], is seen for $R_m=1.75$ ($\gamma=55.0°$). We observe even larger changes in the rearrangement process when we increase the wavelength ratio further to $R_m=2.0$ ($\gamma=60.0°$).

In this instance, after the illumination, the imprinted TP split up in a highly ordered fashion to eventually form an "alternating-fishbone" pattern along the symmetry axis [Fig. 2(c)]. We observe a concerted, asymmetric rearrangement in which the bright stripes break up on one side of the horizontal midline [Fig. 2(c), column 2]. This temporary symmetry loss slowly gives way to a subsequent rearrangement in which the ends of the bright stripes realign to form a stable, "alternating-fishbone" configuration [Fig. 2(c), column 4].

During this rearrangement scenario, the initial pattern, which has translation, horizontal line reflection, and glide reflection symmetries, breaks up and readjusts to a structure that exhibits only translation and glide reflection symmetries. The overall symmetry change can also be analyzed in the context of *frieze patterns*, two-dimensional patterns periodic in one direction, which play a role in architecture and decorative art. All such patterns can be classified into seven distinct groups based on the combination of symmetries they exhibit. Employing the apt notation suggested by Conway (one of the many notations proposed for these groups), we can formulate this "fishbone-to-alternating-fishbone" pattern rearrangement as "jump" → "step". Here "jump" corresponds to a pattern with translation, horizontal line reflection, and glide reflection symmetries (e.g., "< < <") and "step" to a pattern with translation and glide reflection only (e.g., "/ \ / \ / \"). More detailed descriptions of frieze patterns with examples can be found in Refs. [16,17]. Similar structures have also been observed in thin block copolymer films [18] and in Rayleigh-Bénard convection patterns [19].

Increasing the wavelength ratio along the line of vertices leads to a second scenario, which results in a configuration with only translational symmetry. When $R_m=2.6$ ($\gamma=67.5°$), after the illumination is turned off, the breakup yields asymmetric pairs of bright half-lines, one bending around another [Fig. 2(d)].

Further increase of R_m eventually leads back to the symmetry-preserving rearrangement dynamics. For $R_m\geq 3.0$ [$\gamma\geq 70.5°$, Figs. 2(e)–2(h)], after the illumination is turned off, the vertices narrow while the ends of the stripes remain attached and line up in parallel. For these large R_m values, the patterns remain repetitive, with structures resembling a row of "tuning forks" in the horizontal midsection. Above a certain wavelength ratio, however, the TP undergo symmetry loss during reconfiguration. Figure 2(h) ($R_m=6.0$, $\gamma=78.5°$) shows a typical scenario for this wavelength ratio, in which the defects are different from those observed during the asymmetric phase of the rearrangement in the vicinity of $R_m=2.0$. At large angles, breakup of stripes occurs frequently at random locations on both sides of the axis, resulting in structures with no translational or reflection symmetry.

To qualitatively characterize the relaxation process, we calculate one-dimensional Fourier transforms of snapshots taken along the axis of symmetry. For each experiment shown in Fig. 2, we obtain a series of seven Fourier spectra, which are presented as a three-dimensional surface in Fig. 3. Note that instead of the usual wave number, we use the wavelength divided by the intrinsic wavelength (λ/λ_P), hence our x-axis is scaled by the pattern's natural wavelength.

When $R_m=1.5$, the Fourier analysis yields a single peak at $1.5\lambda_P$, which grows until the TP becomes stationary [Fig. 3(a)]. A similar surface is obtained when $R_m=1.75$, with a peak located at the corresponding wavelength [Fig. 3(b)], even though the TP breaks up at a few locations along the symmetry axis. This loss of symmetry, however, has no effect on the Fourier spectra, as it leaves the spatial repeat distance along the line of vertices essentially unchanged.

The Fourier analysis also successfully grasps the main characteristics of the complex dynamics seen for $R_m=2.0$ [Fig. 3(c)]. At $t=0$, representing the imprinted structure, the highest amplitude mode is located at $2\lambda_P$. This mode gradually diminishes to give way to another mode at the intrinsic wavelength λ_P. Increasing R_m leads to the asymmetric final pattern discussed above, which has a qualitatively different Fourier spectrum [Fig. 3(d)]. Supporting the visual assessment, we obtain a bimodal spectrum with peaks at $2.4\lambda_P$ and $1.2\lambda_P$.

In the $6.0\geq R_m\geq 3.0$ parameter range, the spectra are again unimodal. Similar to the $R_m\leq 1.75$ regime, the peaks are located at their corresponding λ_m wavelengths.

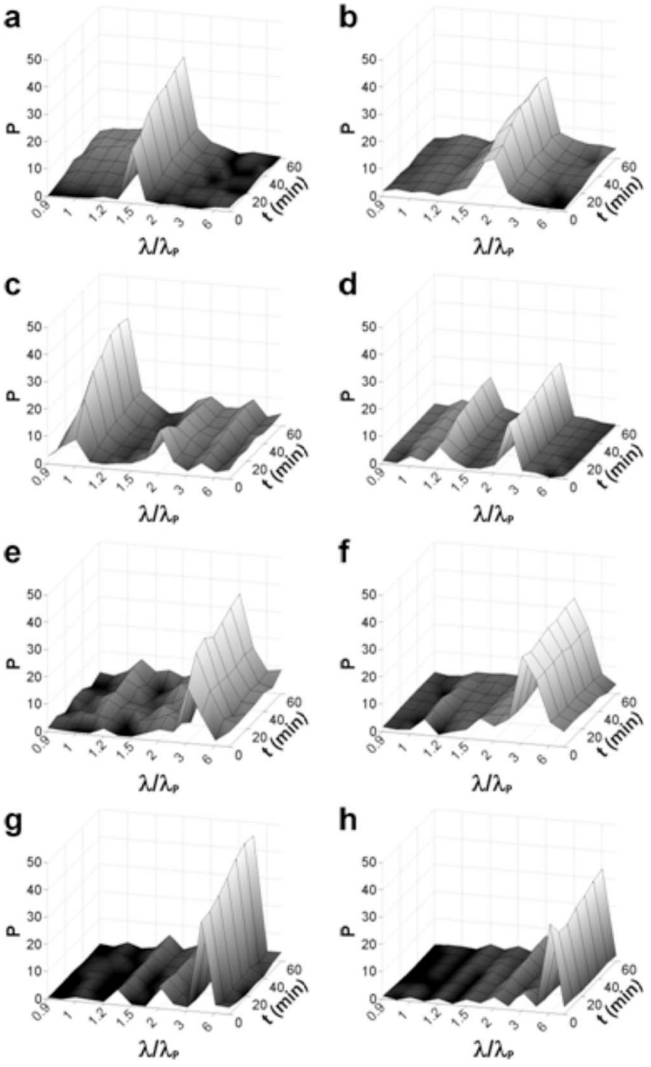

FIG. 3. Self-rearrangement of TP represented as consecutive 1D Fourier spectra calculated along the symmetry axis from snapshots shown in Fig. 2. $R=1.0$, (a) $R_m=1.5$, (b) $R_m=1.75$, (c) $R_m=2.0$, (d) $R_m=2.6$, (e) $R_m=3.0$, (f) $R_m=3.5$, (g) $R_m=4.0$, and (h) $R_m=6.0$.

To gain a more general understanding of this type of self-rearrangement process, we carry out experiments at both lower and higher initial concentrations of iodine while keeping all other parameters unchanged. We confine our attention to the cases $R_m=2.0$ and 3.0. For the latter wavelength ratio, the experiments reveal only readjustment processes similar to that shown in Fig. 2(e). For $R_m=2.0$, however, two distinctly different scenarios emerge. In one, involving lower concentrations of iodine, the readjustment process preserves the symmetry, as seen in both the snapshots and the Fourier spectra [Figs. 4(a) and 4(c)]. In the other scenario, at higher iodine concentrations, the initial and final patterns share the same symmetries (reflection and translation), but their structures differ substantially. The imprinted TP break up on both sides of the horizontal midline, leading to a "dotted-fishbone" configuration made up of a regular array of spots replacing the vertices [Fig. 4(b)]. The Fourier analysis yields one major peak at $2\lambda_P$ that corresponds to the wavelength of the imposed mask, λ_m ($R_m=2.0$).

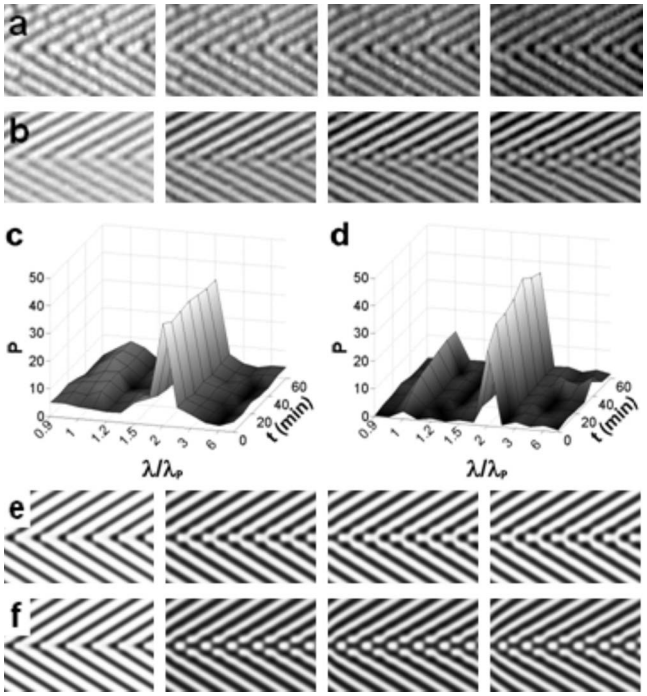

FIG. 4. Relaxation of patterns after illumination and corresponding Fourier spectra, $R=1.0$, $R_m=2.0$. Experimental results: (a, c) $[I_2]_0=0.2$ mM, (b, d) $[I_2]_0=0.4$ mM, and corresponding results of simulations: (e) $b=0.20$, (f) $b=0.30$. Additional parameters are given in the Experimental and Simulations sections, respectively. Snapshots in each row are taken 0, 10, 30, and 60 min after the illumination is switched off. Image size as in Fig. 2. Times for corresponding numerical snapshots: 0, 10, 30, and 60 t.u.

Results on Turing patterns evolving from forced, fishbone-shaped initial arrangements with $R=2.0$ are presented in Fig. 5. In agreement with Ref. [12], outside the horizontal midsection each bright band splits into two to adapt to the system's natural wavelength. Similar dynamics shapes the pattern along the symmetry axis in the first two cases where $R_m=3.0$ and 4.0, respectively. The splitting, however, is asymmetric, which leads to segmentation on the concave side of the bright stripes established during forcing. Notice that these are also symmetry-preserving transitions, leaving each initial translation vector unchanged. Increasing R_m also results in the aforementioned segmentation, but, for higher wavelength ratios, this process already starts before the illumination is turned off. This premature segmentation significantly affects the final configurations, which resemble those for $R=1$, $R_m>2.6$. The Fourier spectra nicely demonstrate how the forcing mode quickly diminishes after the illumination is turned off while others take over. For $R_m=3.0$ and $R_m=4.0$ the TP with altered wavelengths yield bimodal Fourier spectra [Figs. 5(e) and 5(f)].

In a final set of experiments we keep γ constant at 60° and vary the wavelength of forcing λ_F (Fig. 6). When $R=3.0$, the imposed pattern has a wavelength of $1.5\lambda_P$ outside the horizontal midsection. Consequently, a zigzag pattern develops during the relaxation [Fig. 6(a)]. In the horizontal midsection, the symmetric rearrangement process is hindered by the adjacent erratic pattern development. As a result, the

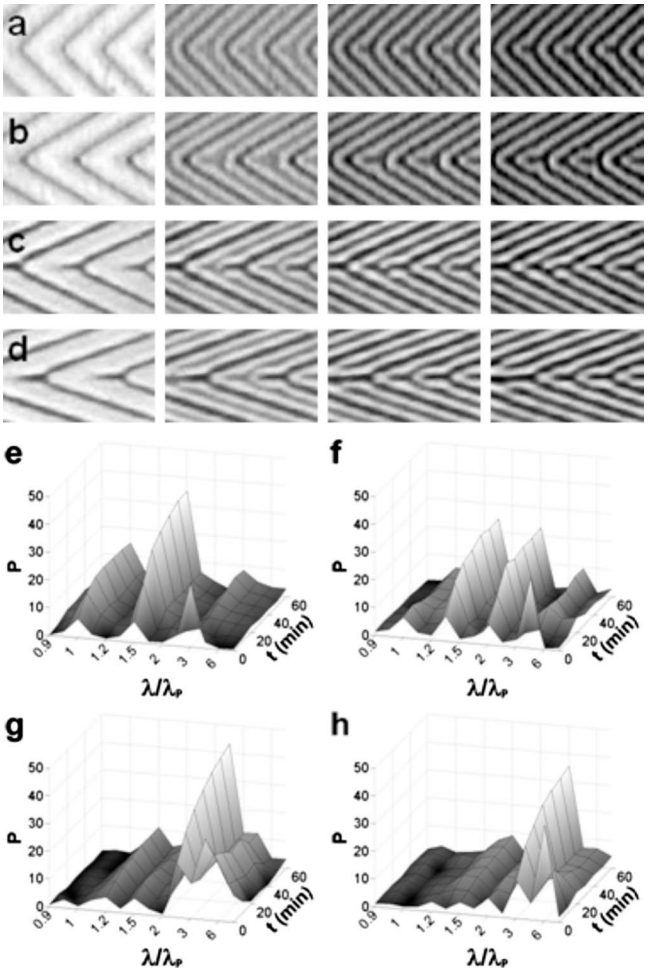

FIG. 5. Pattern relaxation and corresponding Fourier spectra; $R=2.0$, (a, e) $R_m=3.0$, (b, f) $R_m=4.0$, (c, g) $R_m=4.7$, and (d, h) $R_m=6.0$. Snapshots in each row are taken 0, 10, 30, and 60 min after the light is turned off. Image size as in Fig. 2.

Fourier mode [Fig. 6(d)] at $3\lambda_P$ loses its initial dominance but remains significant while others at $1.5\lambda_P$ and λ_P grow before they establish their steady levels. For $R_m=5.0$, after the illumination is turned off the forced TP outside the axis of symmetry ($R=2.5$) split in two [Fig. 6(b)]. Along the line of vertices, the TP lose their periodicity and establish an aperiodic configuration, which appears in the form of a quickly diminishing mode at $5\lambda_P$ that gives way to a group of low amplitude modes in the vicinity of λ_P. Further increase in the wavelength leads to the scenario presented in Fig. 6(c). When $R_m=8.0$ and 4.0, the relaxation fails to yield a steady final pattern within 60 min, though the pattern does stabilize after about 120 min [12]. Along the symmetry axis we observe rapidly decreasing modes around $8\lambda_P$ with simultaneous growth of the mode representing the natural wavelength (λ_P) of the prevailing labyrinthine TP. Outside the horizontal midsection, the pattern looks somewhat less erratic, as it is mainly composed of stripes that roughly follow the orientation of the mask.

IV. SIMULATIONS

We employ the two-variable Lengyel-Epstein model that incorporates the effect of illumination [6]:

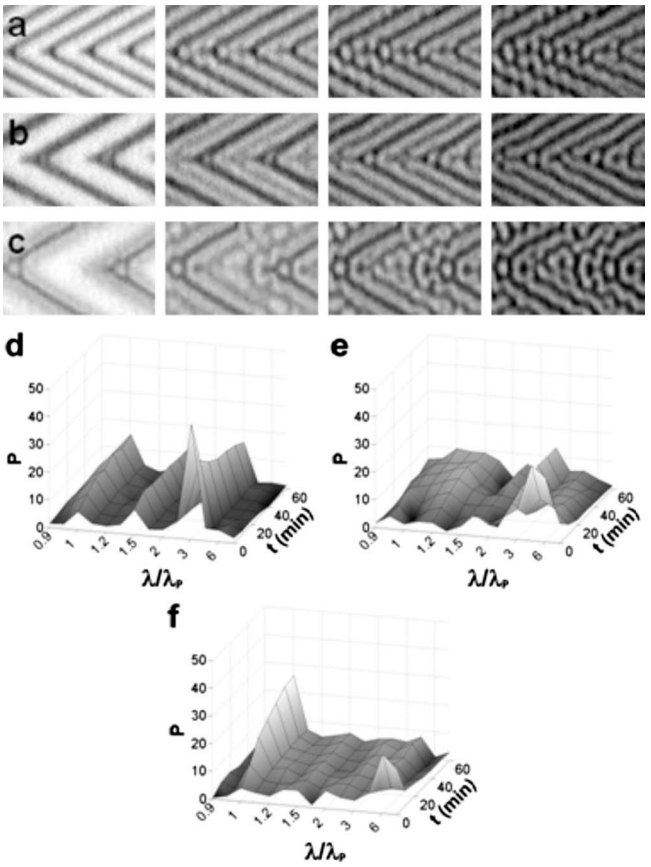

FIG. 6. Pattern development after illumination and corresponding power spectra; (a, d) $R=1.5$, $R_m=3.0$; (b, e) $R=2.5$, $R_m=5.0$, (c, f) $R=4.0$, $R_m=8.0$. Snapshots in each row are taken 0, 10, 30, and 60 min after the light is turned off. Image size as in Fig. 2

$$\frac{\partial u}{\partial t} = a - u - 4\frac{uv}{1+u^2} - w(x,y) + \nabla^2 u$$

$$\frac{\partial v}{\partial t} = \sigma\left[b\left(u - \frac{uv}{1+u^2} + w(x,y)\right) + d\nabla^2 v\right], \qquad (1)$$

where u and v are the dimensionless concentrations of iodide and ClO_2^- ions, respectively; a, b, c, d, and σ are dimensionless parameters, and w denotes the rate of the photochemical reaction. Unless otherwise stated, we assign $a=12$, $b=0.25$, $d=1$, and $\sigma=50$, which yields labyrinthine TP similar to those seen in experiments. The model equations are solved numerically with the Euler method with fixed time step 0.001 time units (t.u.) and zero-flux boundary conditions. For initial conditions, we set both variables to their unstable steady-state values and add a small perturbation to u at each grid point. The spatial modulation is controlled by w, defined as $w_{ij}=w_0 m_{ij}$, where w_0 is a constant set so that $w_{max}=1.5$, and m is a matrix with elements $0 \le m_{ij} \le 1$ obtained by rescaling the mask used in our experiments. After 20 t.u. the imprinted patterns become stationary. We then set $w_0=0$ and continue with simulation of the subsequent relaxation dynamics.

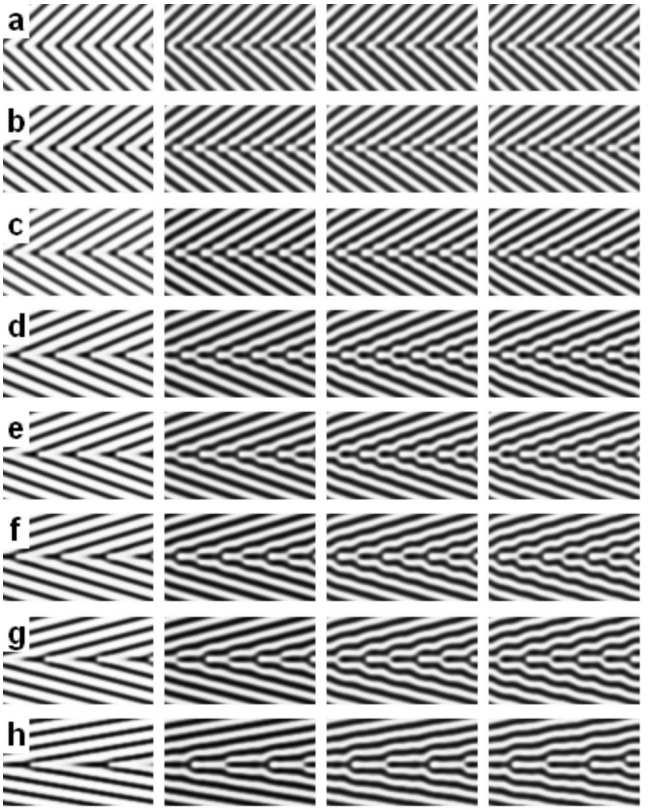

FIG. 7. Simulations of pattern development $R=1$ and (a) $R_m=1.5$, (b) $R_m=1.75$, (c) $R_m=2.0$, (d) $R_m=2.6$, (e) $R_m=3.0$, (f) $R_m=3.50$, (g) $R_m=4.0$, and (h) $R_m=6.0$. Snapshots in each row are taken 0, 10, 30, and 60 time units after the illumination is turned off. Further parameters are given in the Simulation section.

V. NUMERICAL RESULTS

Results of simulations for $R=1.0$ (Fig. 7) are qualitatively similar to those observed in experiment (Fig. 2). When we change the angle γ, the self-rearrangement of TP is reproduced by our simulations. The numerical simulations confirm that the translation and reflection symmetries of the patterns are preserved in most cases. Only when $\gamma=60°$ [$R_m=2.0$, Fig. 7(c)] is an "alternating-fishbone" pattern with translation and glide reflection symmetries obtained, in agreement with the experiments [Fig. 2(c)]. The simulations also reproduce the changes in pattern formation when the iodine concentration is varied. [Figs. 4(e) and 4(f)].

For $\gamma=67.5°$ [$R_m=2.6$, Fig. 7(d)] the simulations give patterns that are somewhat different from the patterns observed in experiment, as the horizontal line symmetry is preserved during the relaxation period shown in Fig. 7(d). However, with time this symmetry is lost. The only difference is that in the simulations the symmetry loss requires more time than in the experiments.

For $R=2.0$ the results of simulations (Fig. 8) and experimental results (Fig. 5) are in good agreement when forcing by illumination is applied. When $R_m=3.0$ [Fig. 8(a)] the new pattern that replaces the one imposed by illumination remains stable and preserves the translational vector of the imprinted TP. For higher values of R_m, pattern readjustment

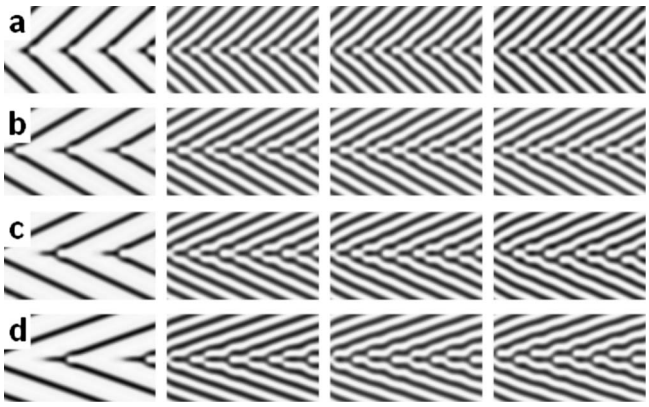

FIG. 8. Simulations of pattern development; $R=2.0$, (a) $R_m=3.0$, (b) $R_m=4.0$, (c) $R_m=4.7$, and (d) $R_m=6.0$. Other parameters and times of snapshots as in Fig. 7.

along the axis of symmetry continues even after the arrangements found stable in experiment are reached. When $R_m=4.0$, the stripes remain unbroken, but the string of alternating-length nibs along the symmetry axis changes as the length of the nibs become equal and the distance between them reaches a constant value [Fig. 8(b)]. Similar readjustment dynamics shapes the TP at larger R_m. However, in this case the rearrangement eventually leads to the breakup of stripes in the horizontal midsection [Figs. 8(c) and 8(d)].

Keeping γ constant at 60° and changing the wavelength of forcing, λ_F, gives results (Fig. 9) that are in partial agreement with our experimental results (Fig. 6). When $\lambda_F=1.5\lambda_P$ ($R_m=3.0$), spots appear along the line of vertices after the forcing is turned off. The imprinted pattern outside the symmetry axis remains stable instead of zigzagging. Similar behavior of imprinted stripes with wavelength $1.5\lambda_P$ was reported in Ref. [12] and linked to the effect of strong illumination, which suppressed the initial random perturbation. When $\lambda_F=2.5\lambda_P$ ($R_m=5.0$), the imprinted TP becomes erratic along the symmetry axis, and the resulting configuration shares only slight resemblance with the experimental findings. Off the axis, however, the imposed stripes split as seen in experiment. When $\lambda_F=4.0\lambda_P$ ($R_m=8.0$), spots appear during forcing in areas where w_{ij} is near or equal to zero. Spots also develop during illumination in the experiments, but only along the symmetry axis [Fig. 6(c)]. In the absence of forcing, the unstable TP rearranges to a labyrinthine con-

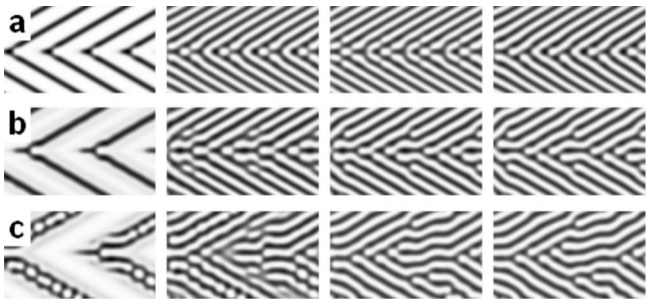

FIG. 9. Simulations of pattern development; $\gamma=60°$, (a) $R=1.5$, $R_m=3.0$, (b) $R=2.5$, $R_m=5.0$, (c) $R=4.0$, $R_m=8.0$. Remaining parameters and times of snapshots as in Fig. 7.

figuration consisting of stripes that preserve the orientation attained during forcing.

VI. CONCLUSIONS

Our results show that the fishbonelike configuration achieved by spatial periodic forcing stabilizes striped TP with a broad range of wavelengths along the line of vertices. The periodicity in the horizontal midsection is often achieved by a concerted self-readjustment process in which a highly regular row of nibs develops. There are a few exceptions, when after the forcing the pattern development takes different paths, leading to sometimes unexpected, symmetric configurations such as alternating-fishbone, dotted-fishbone, or structures composed of alternating length nibs.

Numerical results obtained with a simple two-variable model reproduce the experimental findings rather well and mimic many of the complex self-rearrangement processes when the ratio of the forcing and natural pattern wavelengths is relatively small. When the forcing wavelength is significantly larger than the natural pattern wavelength, the model gives only semiqualitative agreement. This discrepancy is likely due to the presence of noise in the experiments, which is difficult to reproduce in simulations.

These findings complement previous results regarding the relaxation of striped TP with wavelengths different from the pattern's intrinsic wavelength [12] and provide more insights into self-adjustment dynamics in naturally occurring labyrinthine arrangements. The stable configurations presented here can also be regarded as possible building blocks of patterns with complex planar symmetry and might be used in producing TP made up of a variety of polygons. For example, knowledge of the range of stable angles at which stripes can meet might enable one to create arrangements of polygonal TP that tile the plane or form a "Turing quasicrystal." Also, theoretical work [20] suggests that bistable reaction-diffusion systems could prove useful in building a chemical memory device, and a crude experimental implementation [21] was carried out in a photosensitive reaction-diffusion system in which a localized Turing state coexists with a spatially uniform steady state. Again, knowing what kinds of structures can persist after the illumination is removed will be of considerable importance in expanding the capabilities of such devices.

ACKNOWLEDGMENT

This work was supported by Grant No. CHE-0615507 from the National Science Foundation. S.A. was supported by REU Grant No. CHE-0552767 from the National Science Foundation.

[1] A. M. Turing, Philos. Trans. R. Soc. London, Ser. B **237**, 37 (1952).
[2] V. Castets, E. Dulos, J. Boissonade, and P. De Kepper, Phys. Rev. Lett. **64**, 2953 (1990).
[3] P. De Kepper, I. R. Epstein, K. Kustin, and M. Orbán, J. Phys. Chem. **86**, 170 (1982).
[4] I. Lengyel, G. Rábai, and I. R. Epstein, J. Am. Chem. Soc. **112**, 4606 (1990).
[5] A. P. Muñuzuri, M. Dolnik, A. M. Zhabotinsky, and I. R. Epstein, J. Am. Chem. Soc. **121**, 8065 (1999).
[6] A. K. Horváth, M. Dolnik, A. P. Muñuzuri, A. M. Zhabotinsky, and I. R. Epstein, Phys. Rev. Lett. **83**, 2950 (1999).
[7] M. Dolnik, I. Berenstein, A. M. Zhabotinsky, and I. R. Epstein, Phys. Rev. Lett. **87**, 238301 (2001).
[8] I. Berenstein, L. Yang, M. Dolnik, A. M. Zhabotinsky, and I. R. Epstein, Phys. Rev. Lett. **91**, 058302 (2003).
[9] L. Yang, M. Dolnik, A. M. Zhabotinsky, and I. R. Epstein, Chaos **16**, 037114 (2006).
[10] D. G. Míguez, V. Pérez-Villar, and A. P. Muñuzuri, Phys. Rev. E **71**, 066217 (2005).
[11] D. G. Míguez, M. Dolnik, A. P. Muñuzuri, and L. Kramer, Phys. Rev. Lett. **96**, 048304 (2006).
[12] I. Berenstein, M. Dolnik, A. M. Zhabotinsky, and I. R. Epstein, J. Phys. Chem. A **107**, 4428 (2003).
[13] M. C. Cross, M. Louie, and D. Meiron, Phys. Rev. E **63**, 045201(R) (2001).
[14] R. A. Segalman, Mater. Sci. Eng. R. **48**, 191 (2005).
[15] *Handbook of Preparative Inorganic Chemistry*, 2nd ed., edited by G. Brauer (Academic, New York, 1963).
[16] J. H. Conway, H. Burgiel, and C. Goodman-Strauss, *The Symmetries of Things* (A. K. Peters Ltd., Wellesley, MA, 2008).
[17] J. H. Conway, P. Doyle, J. Gilman, and B. Thurston, *Geometry and the Imagination*, p. 56, http://www.math.dartmouth.edu/~doyle/docs/gi/gi.pdf
[18] A. Horvat, G. J. A. Sevink, A. V. Zvelindovsky, A. Krekhov, and L. Tsarkova, ACS Nano **2**, 1143 (2008).
[19] S. W. Morris, E. Bodenschatz, D. S. Cannell, and G. Ahlers, Phys. Rev. Lett. **71**, 2026 (1993).
[20] P. Coullet, C. Riera, and C. Tresser, Chaos **14**, 193 (2004).
[21] A. Kaminaga, V. K. Vanag, and I. R. Epstein, Angew. Chem., Int. Ed. **45**, 3087 (2006).